Beam-steering improvements using agile beam radiating surfaces

B.Jecko[(1)] M. Majed [(1,2)] M. Rammal [(2)] H. Abou Taam [(3)] J. Andrieu [(1)]

[(1)] XLIM, Limoges/87060, France.
(Email: mohamad.majed@xlim.fr)
[(2)] ITHPP, Thegra/46500, France.
[(3)] Lebanese university, Beirut/1003, Liban.

Abstract: **The beam-steering procedure is usually performed using the AESA (Agile Electronically Scanned Array) technique which presents some limitations.**

Therefore, the question is: Is the array technique the best solution to perform the beam-steering?

To answer this question, a rigorous approach has been performed and after, sampling procedures were applied to introduce the agility. The use of a Dirac Comb sampler leads to the array solution (AESA), while a more accurate sampling procedure based on rectangular functions leads to an intrinsically better design than the array, based on "pixels". The advantage is highly significant in order to obtain beams corresponding to high steering angles; particularly wide frequency band solutions are obtained with pixelization lobes more than 6 dBi lower than AESA grating lobes.

Finally, only this new approach is optimized to offer a highly efficient solution for Telecommunications, Radar and Electronic Warfare applications.

AESA, ARMA, Beam-steering.

I. INTRODUCTION

The Array Technique was born when the dipole radiated field expression was elaborated by H.R. Hertz in 1885. The beam agility was introduced later with BFN (Beam Forming Network) manufacturing techniques and has led to a well-known approach called AESA (Agile Electronically Scanned Array). This technique presents some limitations for beam-steering applications: Surface efficiency, frequency bandwidth, coupling effects, high angle scanning limitation, grating lobe levels… To overcome these limitations a new approach called ARMA (Agile Radiating Matrix Antenna).was proposed [1] and exhibited always better results than AESA particularly for beamforming [2] and beam-steering [1]. The first aim of this paper is to explain these better results by introducing a rigorous approach, followed by two different sampling techniques. One leads to AESA and the other one, introducing a more accurate sampling technique, leads to ARMA. Finally only the ARMA technique is performed to optimize the beamforming with 2 different constraints: "Wide band" and "high steering angles".

II. THE RIGOROUS APPROACH:

Beam-steering procedure needs to generate a lot of Radiation Patterns which are deduced from the EM field expression E(P), (resp H(P)) at any point P in the free space.

This E(P) far field expression is rigorously obtained as a function of the field Es(x,y) located on any closed Radiating Surface "Sc" using the well-known procedure [3]:

- Take Maxwell Equations.
- Establish the equations of propagation (Helmoltz)
- Deduce the free space Green's Function (without the antenna).
- Apply the equivalent principle (Huygens principle) replacing the antenna to be built by currents or surface fields on a closed surface Sc which surrounds the antenna (sometimes the surface of the antenna itself). This surface, is called the "radiating surface".

Finally, [3] the convolution product between the free space Green's function and the fields on the closed radiating surface "Sc" is performed to obtain the radiating integral on Sc (2) .

$$\vec{E}(P) = \frac{jk}{4\pi}\psi(R)(1+cos\theta)\left(cos\varphi\,\overrightarrow{e_\theta} - sin\varphi\,\overrightarrow{e_\varphi}\right) \iint_{Sc} E_S(x,y)e^{i(k\,x\,sin\theta\,cos\varphi\,+\,k\,y\,sin\theta\,sin\varphi)}ds \quad (1)$$

For planar low profile antennas, the closed surface Sc surrounding the antenna is chosen to be a flat parallelepiped-shaped one (fig 1), where the main part of the energy flows through the upper part of Sc called S. The radiated energy flowing through the lateral surface is neglected, then Sc≃S.

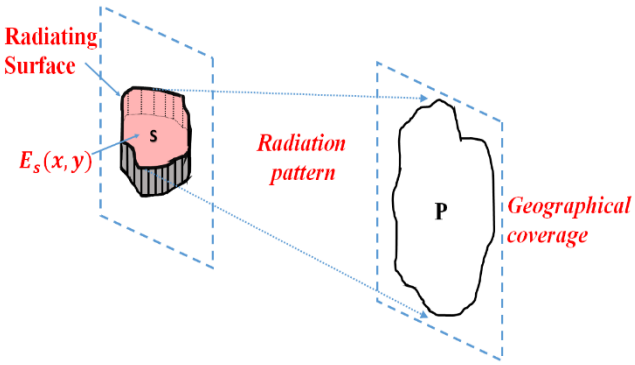

Figure 1: Radiation pattern obtained directly from the radiating surface limited to its upper part.

The same kind of approximation is used for the study of aperture antennas, which leads to the same equation; then (1) is often called the "aperture" radiating surface integral [4]. Furthermore, the Es field is equal to zero outside the S surface, so the integral can be extended to the infinity and the field expression becomes a *Spatial Fourier Transform (SFT)*.

$$\vec{E}(P) = \mathrm{K}\,.\,SFT \qquad (2)$$

With:

$$SFT = \iint_{\infty} E_S(x,y)e^{i(k\,x\,sin\theta\,cos\varphi\,+\,k\,y\,sin\theta\,sin\varphi)}ds \qquad (3)$$

SFT is a *Spatial Fourier Transform* and: $\psi(R) = \frac{e^{jkR}}{R}$

This integral shows that the radiated field E(P) is approximately the 2D *Spatial Fourier Transform* (*SFT*) of the field $E_s(x,y)$ defined on the radiating surface S (Figure 1). The approximation is very light because it is only due to the amplitude term (1 + *cos* θ) in (eq 1) which modifies only the amplitude.

III. Ideal Beam-Steering Procedure

The previous relation E(P) = K × *SFT* (Es) leads to the beam-steering procedure illustrated on a simple example. Let us consider a planar uniform rectangular radiating surface (Figure 2) characterized by a surface field Ex constant in modulus and phase. The radiation pattern of such surface has a "*Sinc*" shape (*SFT*) with a maximum in the axial direction (Figure 2).

If we apply the following FT property:

Multiplying the rectangular function by exp(αx) introduces a shift on the *SFT* ; then the *FT* of (Rectangular Function × $e^{(j\alpha x)}$) exhibit a maximum translated in the θ_{max} direction given by : θ_{max} = - *Arcsin* (λ α / 2π) (Figure 3).

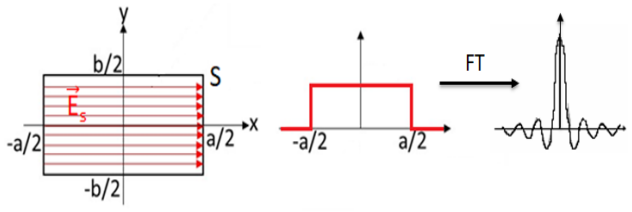

Figure 2: A planar uniform rectangular radiating surface and its FT.

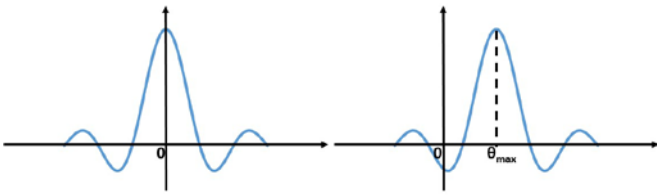

Figure 3: Illustration of beam translation to the θmax position.

The ideal beam-steering procedure obtained with a rectangular radiating surface 4λ x λ/2 is presented for different steering angles on the blue curves of Figure 4 and Figure 9.

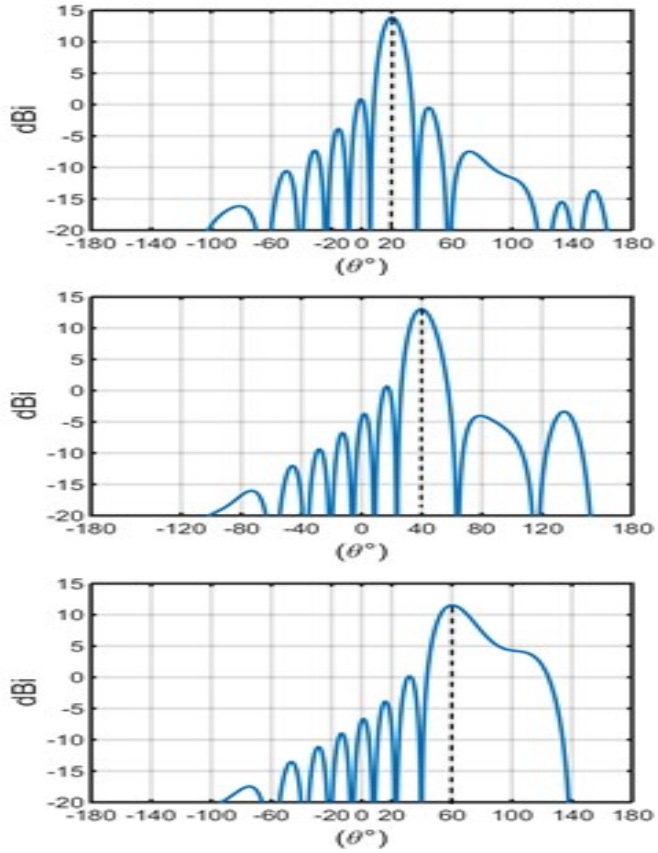

Figure 4: Ideal beam-steering for 20° 40° and 60°.

Side lobes are only due to the whole antenna limitation in the x direction.

IV. Introduction of the Beam Agility

Beam-steering procedure requires a lot of radiation patterns to perform the beam agility; the Es surface field must be sampled to be able to generate beams in many directions.

Consequently, the previous approach becomes no longer a rigorous one. Two sampling techniques are proposed:

1. The most basic sampling procedure to sample an Es(x,y) field is to use a Dirac comb [3].

$$\widetilde{E_s}(x,y) = \sum_i \sum_j E_S(x_i,y_j)\,\delta_{x_i,y_i}(x,y)$$

Introducing this formula in the equation n°1 leads to the following expression:

$$E(P) = K \sum_i \sum_j E_s(x_i, y_j) e^{j(kxsin\theta cos\phi + kysin\theta sin\phi)} \text{dxdy}$$

The radiated field E(P) is the sum of contributions of punctual sources located at (x_i, y_j) coordinates. **That is the array theory:** an antenna called "Array" based on this principle is built with small antennas uniformly distributed on the S surface.

2. Use of the bi-dimensional rectangular function $\prod_{i,j}(x,y)$:

This sampling procedure introduced in Eq n°1 gives:

$$\vec{E}(P) = K \sum_i \sum_j \iint_{s_{i,j}} E_{i,j}(x,y)\, e^{j(kxsin\theta cos\phi + kysin\theta sin\phi)} dxdy$$

$$\vec{E}(P) = K \sum_i \sum_j A_{i,j} \iint_{s_{i,j}} e_{i,j}(x,y) e^{j(kxsin\theta cos\phi + kysin\theta sin\phi)} dxdy$$

With $e_{i,j}(x,y) = 1$ on $s_{i,j}$, = 0 outside.

This expression suggests that the radiated field is the sum of contributions of small "s_{ij}" radiating surfaces generating a constant field "e_{ij}" multiplied by a weighting function $A_{i,j}$.

An antenna surface based on this principle exhibits a lot of joined elements called "pixels" [1] each able to generate a constant field on its surface $s_{i,j}$. All these joined elements can build an antenna, rectangular for example, which looks like a matrix of pixels (Figure 5); hence the name ARMA arises: Agile Radiating Matrix Antenna.

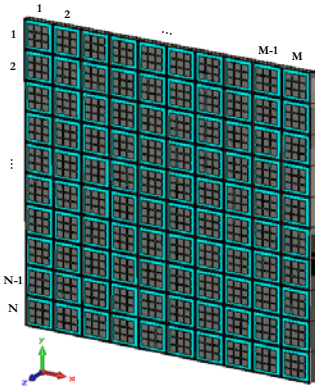

Figure 5: 2D low profile Matrix Antenna called ARMA.

There are no restrictions on the pixels'shapes, therefore many kinds of antennas based on this principle can be manufactured. [1], [5].

V. Pixel Design

The "pixel" [6] [7] is derived from a simple EBG large size antenna (Figure 6a) characterized by a ground plane, an air cavity and a Partially Reflecting Surface (PRS) which is usually a frequency selective surface (FSS) [8] [9] [10] [11]. Metallic walls (Figure 6b) are introduced around the feeding probe (usually a patch) of the EBG antenna [4]. The final structure is shown in figures 7a and 7b. Due to the radially vanishing EBG mode, the surface EM field is almost constant on the top of the pixel (Figure 7c) generating the expected uniform field on the pixel surface [6].

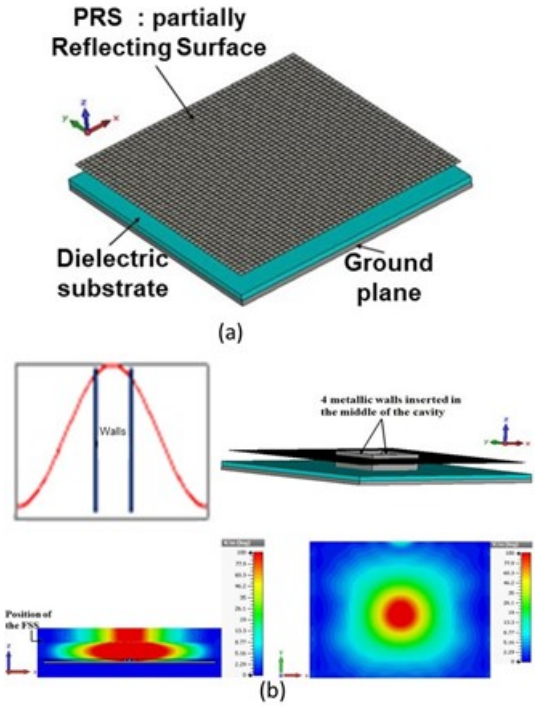

Figure 6: Figure 6 (a) High gain EBG Antenna (b) Vertical metallic walls inside the EBG Antenna and E-field cartography on the radiating surface.

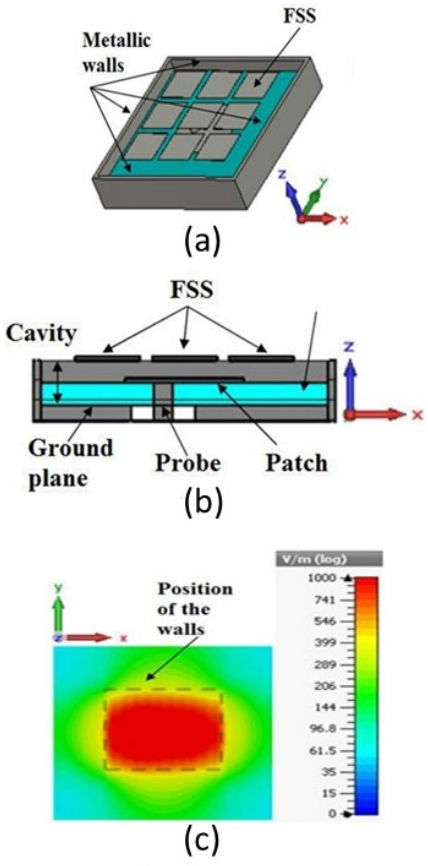

Figure 7: Pixel antenna fed by a patch: (a) Perspective view, (b) Cut view along X-axis, (c) E-field cartography on the pixel-radiating surface.

VI. BEAM-STEERING EFFICIENCY COMPARISON WITH THE TWO APPROACHES:

Let us consider the previous example (Figure 8) sampled in S band by the 2 methods: AESA and ARMA to obtain a 1D beam-steering antenna:

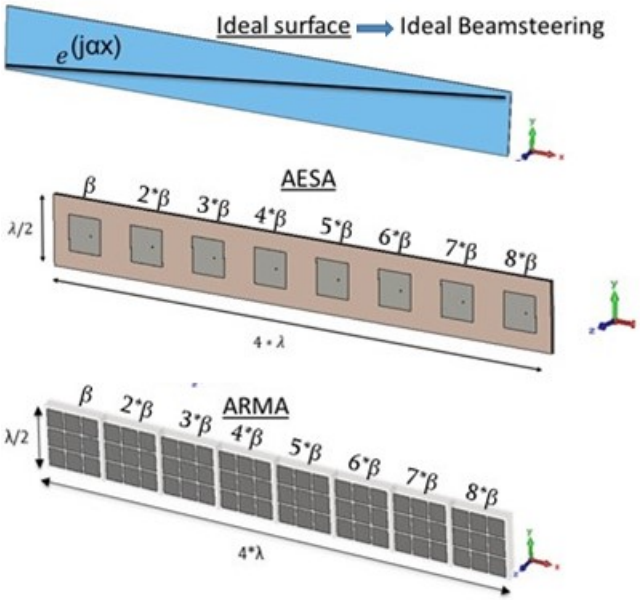

Figure 8: Ideal Beam-steering surface, AESA & ARMA structures.

For small steering angles the radiation patterns obtained by the two 1D antennas are similar and not very far from the ideal case (Figure 9).

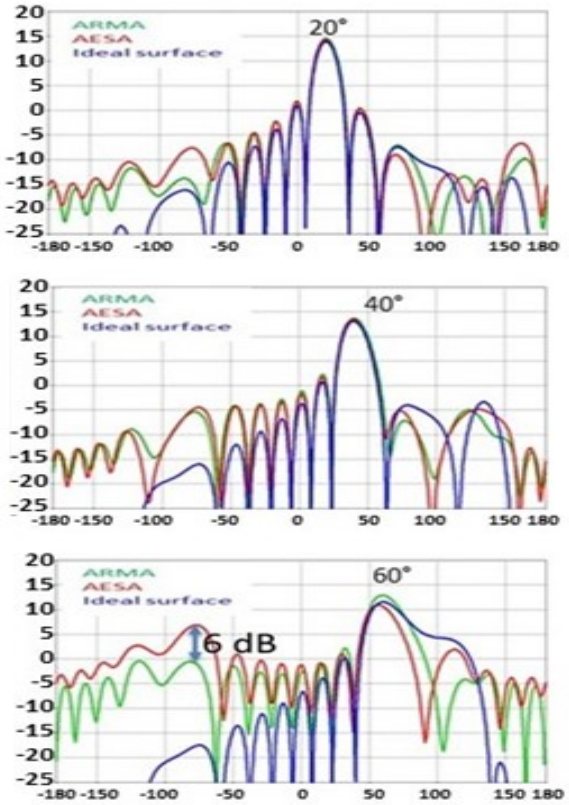

Figure 9: Comparison of ideal surface, AESA and ARMA radiation patterns for a beam-steering procedure in the θ = 20°, 40° and 60° directions.

The result is very different for high scanning angles:

First, it is difficult to obtain good main lobes with AESA solution for directions higher than 50°. Furthermore, grating lobes for AESA and pixelization lobes for ARMA appear and the results are very different from the ideal case (blue curves) for a steering angle of 60° (Figure 9). In addition, there is a big difference (around 6 dBi) between the amplitude of the grating lobe and the pixelization one (Figure 9); this important result is due to the smoothed sampling procedure introduced with ARMA and can be easily generalized to 2D antennas because x and y directions are treated separately:

2D Dirac Comb : AESA	X and Y rectangular function : ARMA
$E(P) \approx FT\{E(x,y) \times \text{Dirac Comb}(x,y)\}$ $E(P) \approx FT\{E(x,y)\} * FT\{\text{Dirac Comb}(x,y)\}$ with : FT{Dirac Comb} is a Dirac Comb convolved with E(x,y) **Grating Lobes**	$E(P) \approx FT\{E(x,y) \times \prod(x,y)\}$ $E(P) \approx FT\{E(x,y)\} * FT\{\prod(x,y)\}$ with : $FT\{\prod\}$ is a *Sinc* convolved with E(x,y) **Smoother pixelization lobes**

VII. WIDE FREQUENCY BAND AND BEAM-STEERING

Many applications, particularly for radars and EW, require "beam-steering on a wide frequency band (≈30%) with high steering angles.

Following the previous results (§ 6) which shows a big difference between ARMA and AESA for high scanning angles, this more difficult problem will be studied only with the ARMA approach which allows a wider active band with the beam-steering procedure.

Let us consider, in S band, a wide band pixel (Figure 10) designed using the technique [6] developped in L band to obtain a wide band (~ 30%) and build a 1D-ARMA with 14 pixels (Figure 11).

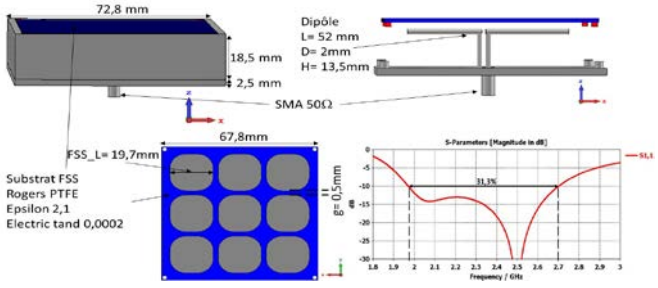

Figure 10: Wide band pixel and S11 parameter as a function of frequency.

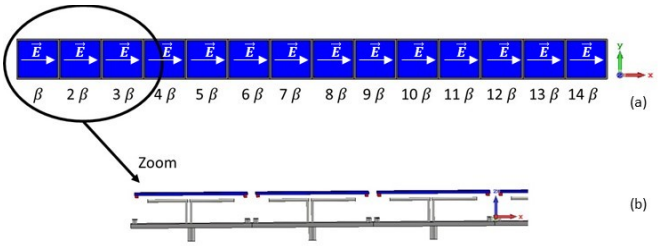

Figure 11: a) ARMA built with the previous pixel; b) cavity view without the lateral walls.

VII.1 Matching Results

In the previous1D ARMA example, the active pixel bandwidths (Figure 12) are near 28% for a beam sent in the axial direction, it is a little bit reduced by the coupling effects to ≈ 23% for a steering angle of 30° and to 27.8% for 60°.

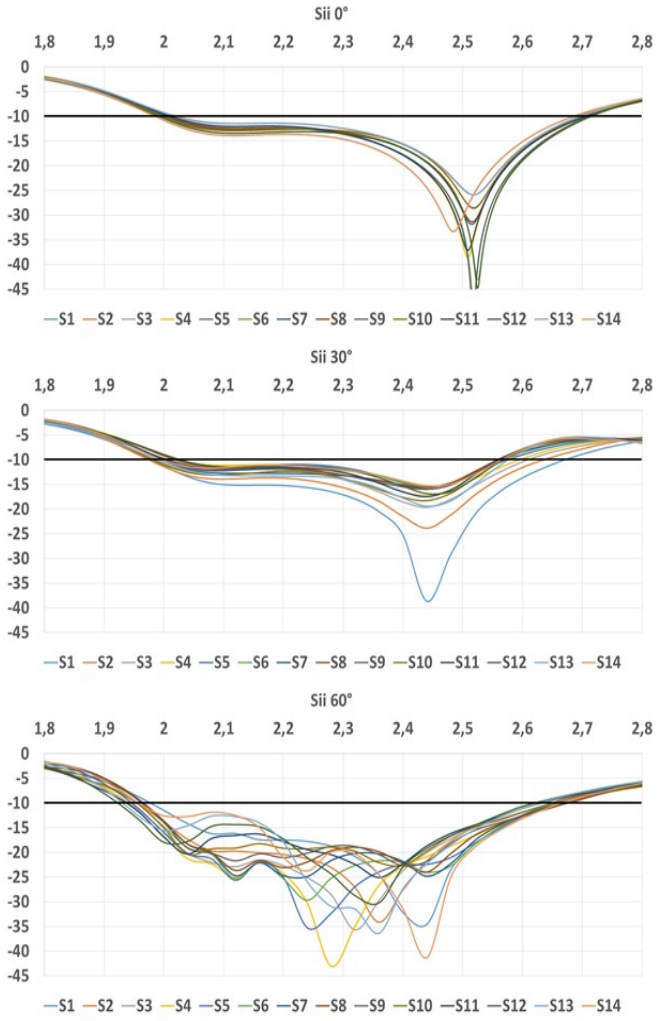

Figure 12: Sii active parameters evolution as a function of the frequency for a beam-steering procedure in the θ = 0°, 30° and 60° directions.

VII.2 Radiation patterns

Considering radiation patterns, the problem is quite different:

- For small beam-steering angles (≤ 30°) the pixelization lobe appears but remains, on all the frequency band, lower than 10dB under the main lobe amplitude (Figure 13) even for the highest frequencies of the band: Wide bandwidth and beam-steering can be performed together. Notice that, already for 30° steering, AESA grating lobe amplitude is at the limit: -10 dB under the main lobe, while ARMA ones are near -17 dBi (Figure 13).

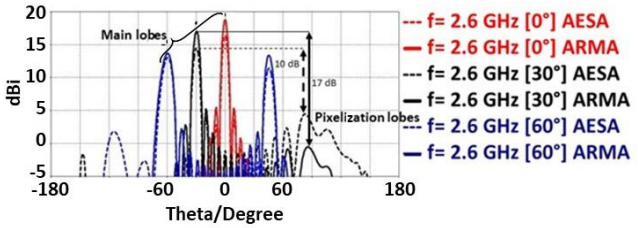

Figure 13: ARMA Radiations patterns evolution as a function of the θ for the highest frequencies of the band in the case of a 0°, 30° and 60° beam-steering and comparison with the array approach(dotted curves).

- For high steering angles, the radiation patterns (Figure 13) are strongly disturbed by the sampling procedure (Fourier transform of a sampled signal). A major problem appears particularly for a 60° beam-steering (Figure 14):

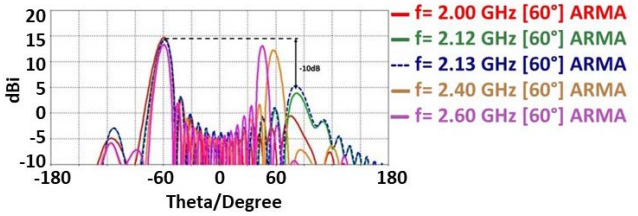

Figure 14: ARMA Realized Gain evolution as a function of θ for different frequencies of the band in the case of a 60° beam-steering.

Pixelization lobe level increases strongly with the frequency (fig14), rendering the solution unusable from 2.13GHz. As said before the specification requires at least a difference of 10 dB in amplitudes between the main lobe and the pixelization one. Consequently, the working band is strongly reduced: ≃ 7.3% for this 60° beam-steering angle.

VIII. Pixelization Lobes Effect Minimization for High Scanning Angles

To cancel the pixelization lobe effect the first idea which comes in mind is to reduce the periodicity of the antenna to shift the pixelization lobe outside the frequency band (cf §3). On the previous example, the pixel length is reduced to 62.5mm shifting the pixelization lobe near 2.6 GHz. The whole matrix E field directivity is then well optimized even for a scanning angle of 60° (Figure 15) where the pixelization lobe is not significant until 2.56 GHz.

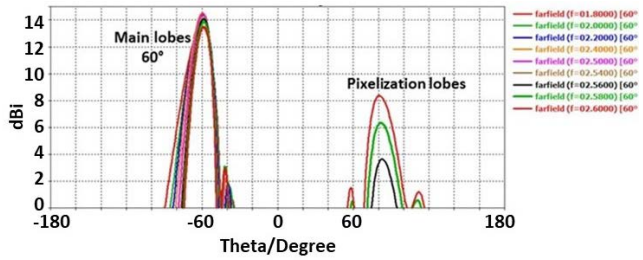

Figure 15: ARMA Radiation pattern evolution as a function of θ for different frequencies of the band in the case of a 60° beam-steering.

Unfortunately, this procedure has a bad effect on the frequency band of the whole matrix antenna, due to the increase of the coupling between smaller pixels. A difference

of 2dB can be observed between the directivity maximum and the realized gain one for 2.56 GHz and a steering angle of 60°, as shown on the figure 16.

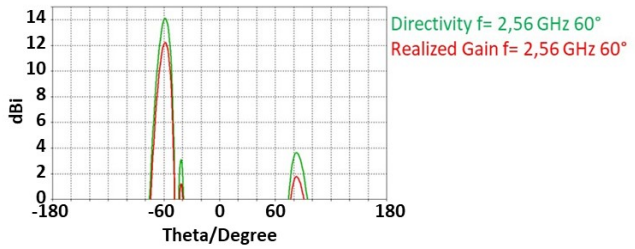

Figure 16: Directivity and Realized Gain comparison for a steering angle of 60° at 2.56GHz.

IX. Conclusion:

Like for beamforming [12], a beam-steering approach applied with an agile radiating surface called ARMA is intrinsically more efficient than AESA particularly because these two approaches are two different sampling methods of a rigorous approach and one is more accurate than the other one.

But any sampling procedure introduces, as the frequency increases, a side lobe (Fourier Transform) which level must remain at least 10 dB lower than the main lobe and thus limits the effective frequency band of the antenna for high steering angles (≃60°).

The previous (case E fig 11) approach can be easily extended to the case of an "oy" polarization of the pixel (case H) which gives similar results. Consequently, circularly polarized pixels [12] can also be used.

In the same way, the beam-steering improvement using a 1D ARMA studied in this paper, can be easily generalized to a 2D beam-steering approach using a 2D ARMA.

References

[1] B. Jecko, E. Arnaud, H. Abou Taam, A. Siblini, "The ARMA concept : Comparison of AESA and ARMA technologies for agile antenna design," Fermat Journal vol 20, 2017.

[2] A. Siblini, E. Arnaud, A. Bellion, H. Abou Taam, B. Jecko, "New Agile Matrix Antenna for Nano-satellite Telemetry Using Bimodal Pattern Reconfiguration," American Journal of Science, Engineering and Technology. Special Issue: Machine Learning in the Internet of Things. Vol. 5, No. 1, 2020, pp. 1-19. doi: 10.11648/j.ajset.20200501.11

[3] L. Schwartz "Methode mathématiques pour les sciences physiques" Collection Enseignement des Sciences – Hermann – Oct. 1997.

[4] P. Vaudon "Antennes à ouverture" http://patrick.vaudon.pagesperso-orange.fr/default.htm

[5] B. Jecko, M. Majed, S. Aija, H. Chereim, A. Siblini, H. Abou Taam, J. Andrieu, M. Lalande, E. Martinod, "Agile Beam Radiating Surfaces," Fermat Journal vol 30, 2018.

[6] M. Rammal, M. Majed, E. Arnaud, J. Andrieu, and B. Jecko, "Small-Size Wide-Band Low-Profile "Pixel Antenna": Comparison of Theoretical and Experimental Results in L Band," International Journal of Antennas and Propagation, vol. 2019, Article ID 3653270, 8 pages, 2019.

[7] M. Majed, Y. Sbeity, M. Lalande, B. Jecko, "Low Profile Circularly Polarized Antenna with Large Coverage for Multi-Sensor Device Links Optimisation," 9th International Conference on Sensor Device Technologies and Applications, Sep 2018, Venice, Italy.

[8] C. Menudier, M. Thevenot, T. Monediere, B. Jecko, "EBG Resonator Antennas," State of Art and Prospects. 6th International Conference on Antenna Theory and Techniques ICATT'07, Sevastopol, the Crimea, Ukraine, September 17-21, 2007.

[9] R.Chantalat, L.Moustapha, M.Thevenot, T.Monediere and B.Jecko, "Low Profile EBG Resonator Antennas," International Journal of Antennas and Propagation. Vol 2009, Article ID 394801, 7Pages.

[10] S. Palreddy, "Wideband Electromagnetic Band Gap (EBG) Structures, Analysis and Applications to Antennas," Dissertation submitted to the faculty of the Virginia Polytechnic Institute and State University in partial fulfillment of the requirements for the degree of Doctor of Philosophy In Electrical Engineering, May 1, 2015.

[11] M. S. Toubet, M. Hajj, R. Chantalat, E. Arnaud, and B. Jecko, "Wide bandwidth, high-gain, and low-profile EBG prototype for high power applications," IEEE Antennas Wireless Propagation Letters, vol. 10, no. 10, pp. 1362– 1365, 2011.

[12] A. Siblilni, B. Jecko, E. Arnaud, "Multimode Reconfigurable Nano-Satellite Antenna for PDTM Application," EUCAP 2017 Paris.